ChemComm

ROYAL SOCIETY OF CHEMISTRY

COMMUNICATION

Published on 22 July 2026
Licence and permissions

Cite this: DOI: 10.1039/d6cc03938c

Received 21st June 2026,
Accepted 22nd July 2026

DOI: 10.1039/d6cc03938c

rsc.li/chemcomm

Phase-preserved fragmentation of bulk WS_2 to nanoparticles in charged water microdroplets

Kausik Kundu, *[a] Sujan Manna, [a] Anirban Som, [a] Anubhav Mahapatra [a] and Thalappil Pradeep *[abc]

Electrospray-generated charged water microdroplets drive stepwise fragmentation of WS_2 sheets of micrometer dimensions into nanoparticles, under ambient conditions. Systematic variation of the tip-to-substrate distance (*L*) and applied voltage (*V*) results in 100-fold lateral size reduction (1–2 μm to ~11 nm), mapped along a (*L*,*V*) matrix. The 2H polymorph is fully retained throughout, as confirmed by HAADF-STEM, HRTEM, and Raman spectroscopy, highlighting charged microdroplets as a platform for sustainable, phase-preserved synthesis of nanomaterials.

Tungsten disulfide (WS_2) in the semiconducting 2H phase is an important layered transition metal dichalcogenide (TMDC) whose properties are strongly governed by dimensionality and morphology.[1] In this thermodynamically stable polymorph, a W atom is coordinated by six S atoms in a trigonal prismatic arrangement, with hexagonal stacking of layers. This is distinct from the metastable 1T polymorph, which adopts an octahedral coordination and exhibits metallic behavior.[2] In reduced dimensions, the 2H polymorph exhibits characteristics that are appealing for applications in catalysis,[3,4] lubrication,[5] and energy storage.[6] However, it is not explored as extensively as its chemical analogue, molybdenum disulfide (MoS_2).[7,8] Despite their promise, direct synthesis of discrete 2H-WS_2 nanoparticles remains challenging because conventional routes often require harsh conditions and typically yield few-layer sheets, defective fragments, or phase-inhomogeneous products.[9] Preserving the 2H polymorph during controlled size reduction remains a synthetic challenge. Conventional strategies like hydrothermal synthesis,[10] sonication-assisted liquid exfoliation,[11] and lithium-ion intercalation[12] convert the semiconducting 2H phase to 1T, introducing basal-plane defects, oxidation, and undesired structural transformations, particularly when strong intercalants, elevated temperatures, or prolonged processing are employed.[13–17] Consequently, there is a clear need for a mild, sustainable, and ambient route that can transform layered WS_2 into nanoparticles while maintaining structural integrity and phase purity.

Charged water microdroplets generated by electrospray provide a distinctive reaction environment, where intense electric fields at the interface,[18,19] rapid solvent evaporation and a large interfacial area can drive rapid transformations under apparently ambient conditions.[20,21] Species such as $OH^{\bullet}$, $H_2O^{+\bullet}$, H_2O_2, and others are present at the interfaces of water microdroplets.[18,22] Such microdroplets have emerged as a versatile medium for accelerating chemical reactions and enabling unusual materials-processing pathways that are inaccessible in bulk solutions.[23–26] We have shown that bulk minerals such as quartz disintegrate to form nanoparticles this way.[23,25,27]

In this communication, we report electrospray-driven, stepwise disintegration of two-dimensional WS_2 sheets into nanoparticles in charged water microdroplets under ambient conditions, *i.e.*, room temperature and atmospheric pressure. The transformation is regulated by the applied voltage and tip-to-substrate distance, enabling systematic control over lateral dimensions and morphological evolution. Remarkably, the 2H crystal phase is retained throughout the process, as confirmed by electron microscopy and Raman spectroscopy. Our study demonstrates the potential of charged microdroplets as a platform for phase-preserved transformation of materials.

Fig. 1 presents the schematic disintegration of bulk WS_2 into nanoparticles *via* ambient charged water microdroplets. Field emission scanning electron microscopy (FESEM) and transmission electron microscopy (TEM) (Fig. 1a–c and Fig. S1) confirm the two-dimensional sheet-like morphology before electrospray. After electrospray at the optimised 5 cm tip-to-substrate distance and 5 kV operating voltage, nanoparticles were formed (Fig. 1d and e). The observed *d* spacing of 0.27 nm corresponds to the (100)/(010) plane of 2H-WS_2; only a three-index notation is used, as is common in the TMDC literature.

[a] *DST Unit of Nanoscience (DST UNS) & Thematic Unit of Excellence (TUE), Department of Chemistry, Indian Institute of Technology Madras (IITM), Chennai 600036, India. E-mail: kausikkundu13@gmail.com, pradeep@iitm.ac.in*
[b] *International Centre for Clean Water, 2nd Floor, B-Block, IIT Madras Research Park, Kanagam Road, Taramani, Chennai 600113, India*
[c] *Centre of Excellence on Molecular Materials and Functions, Department of Chemistry, Indian Institute of Technology Madras, Chennai, 600036, India*

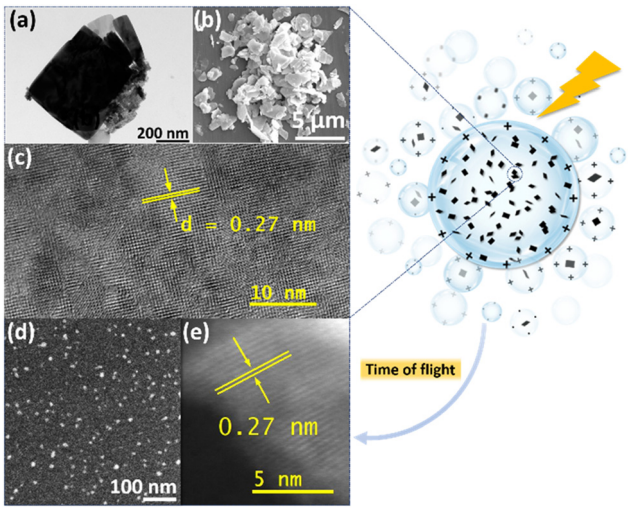

Fig. 1 (right) Schematic diagram of disintegration of 2D WS_2 to nanoparticles in charged water microdroplets. (left) The initial particles before disintegration examined with (a–c) TEM and (b) FESEM and the final nanoparticles examined using (d) HAADF-STEM. The HRTEM images (c–e) show the (100)/(010) plane of WS_2.

It is essential to visualize the product nanoparticles using high-angle annular dark-field scanning transmission electron microscopy (HAADF STEM) in view of its higher contrast (see below). Phase preservation will be discussed later, using Raman spectroscopy. Two-dimensional sheets used for electrospray were synthesised from bulk WS_2 using the water exfoliation method, outlined in the SI. In the disintegration experiment, we used a custom-built electrospray source (Fig. S2) to generate charged water microdroplets containing a fine dispersion of WS_2 sheets of 1–2 μm length, which were sprayed onto substrates. The spray plume emitted from the electrospray tip was visualized with a laser torch. Additional details of the experiment can be found in the SI. Based on trials, an optimal applied voltage (V) of 5 kV was identified for a tip-to-substrate distance (L) of 5 cm for uniform nanoparticle formation. For electron microscopy, the electrospray process was carried out on TEM grids. The TEM image of WS_2 before electrospray reveals a well-defined, sheet-like morphology with lateral dimensions in the micrometer range (Fig. S1c and d), confirming the high-quality water exfoliation of WS_2 yielding thin 2D sheets. 2D projection along the (001) basal plane shows the (100) and (010) edge planes of equal surface energy, representing the thermodynamically stable Wulff construction of square sheets.[28–31] The 2D sheets, characterized by their extended and layered morphology, have been effectively fragmented into uniformly distributed nanoparticles with a particle size distribution of 11.4 ± 2.0 nm (Fig. S3). These particles appear well-dispersed across the TEM grid, indicating effective break-up and dispersion, facilitated by the electrospray process. The nanoparticles exhibit a consistent size, suggesting that charged microdroplets provide a controlled environment for fragmentation and stabilization. The uniformity in particle size and shape aligns with the rapid reactions seen in microdroplet chemistry, where transformations occur within micro to milliseconds as the droplets undergo evaporation and charge-induced fission.

To study the stepwise disintegration, we have changed L and V systematically and constructed a (L,V) morphological matrix of HAADF-STEM images (Fig. 2), particle size distribution (Fig. S3), brightfield-TEM images (Fig. S4) and DigitalMicrograph analysis of the observed d spacings (Fig. S5). Understanding the step-wise disintegration can lead to new areas of application in catalysis, water purification, and environmental technologies. Referring to Fig. 2, starting from (1,1), the path progressed to (5,5), where complete disintegration occurred. WS_2 monolayers appear nearly invisible in bright field-TEM because their thicknesses are in the atomic limit, and phase contrast from such thin specimens is overwhelmed by substrate noise and lens artifacts. In HAADF-STEM, tungsten's very high atomic number (Z = 74) causes massive Rutherford scattering to high angles, producing intense, unambiguous bright spots even for nanoparticles made of monolayers, while the low-Z substrate remains dark.[32,33] This Z^2 contrast mechanism makes HAADF-STEM a definitive tool for imaging in this case. HAADF-STEM images with well-adjusted instrument parameters like electron flux and magnification are presented in Fig. 2 and Fig. S6–S10. At lower applied voltages and shorter tip-to-substrate distances, the electrospray process generates larger microdroplets with weaker internal electrostatic fields, allowing the WS_2 sheets to remain largely intact. As the applied voltage was increased, the electric field strength within the microdroplets intensifies, creating higher electrostatic pressure on the WS_2 sheets and their surrounding ionic atmosphere. Simultaneously, the increased voltage enhances the charge density within each droplet which concentrates the solutes into a progressively smaller volume, resulting in a distorted morphology. Under combined conditions of elevated voltage and extended distance, the accumulated electrostatic stress exceeds the van der Waals binding energy holding adjacent WS_2 layers together, causing the sheets to separate and progressively fragment to individual nanoparticles. At a 4 cm distance and 4 kV applied voltage, co-existence of large sheets, broken sheets and non-broken centres is observed (Fig. S9), which is the transition point, and at (5,5), uniformly distributed nanoparticles are observed. At this (4,4) threshold, the field is just strong enough to detach stacked sheets and start the fragmentation. This is quantitatively supported by the (L,V) matrix of particle size distributions (Fig. S3). The DigitalMicrograph processed (L,V) morphological matrix of high-resolution TEM (HRTEM) images (Fig. S5 and Fig. S6–S10) reveal lattice fringes with a d-spacing in the range of 0.25 to 0.27 nm, consistent with the (100)/(010) planes, and 0.31 to 0.37 nm, consistent with the (004) plane (which depends on the extent of exfoliation) of WS_2, confirming the structural integrity of WS_2 even after disintegration. Strong evidence that transformation, or structural phase change, is the primary fragmentation mechanism is provided by the fact that these two d-spacings are constant over all values (1,1) to (5,5). The preserved d-spacing, which is driven by mechanical cleavage rather than chemical cleavage, also demonstrates that the 2H phase's interlayer stacking geometry

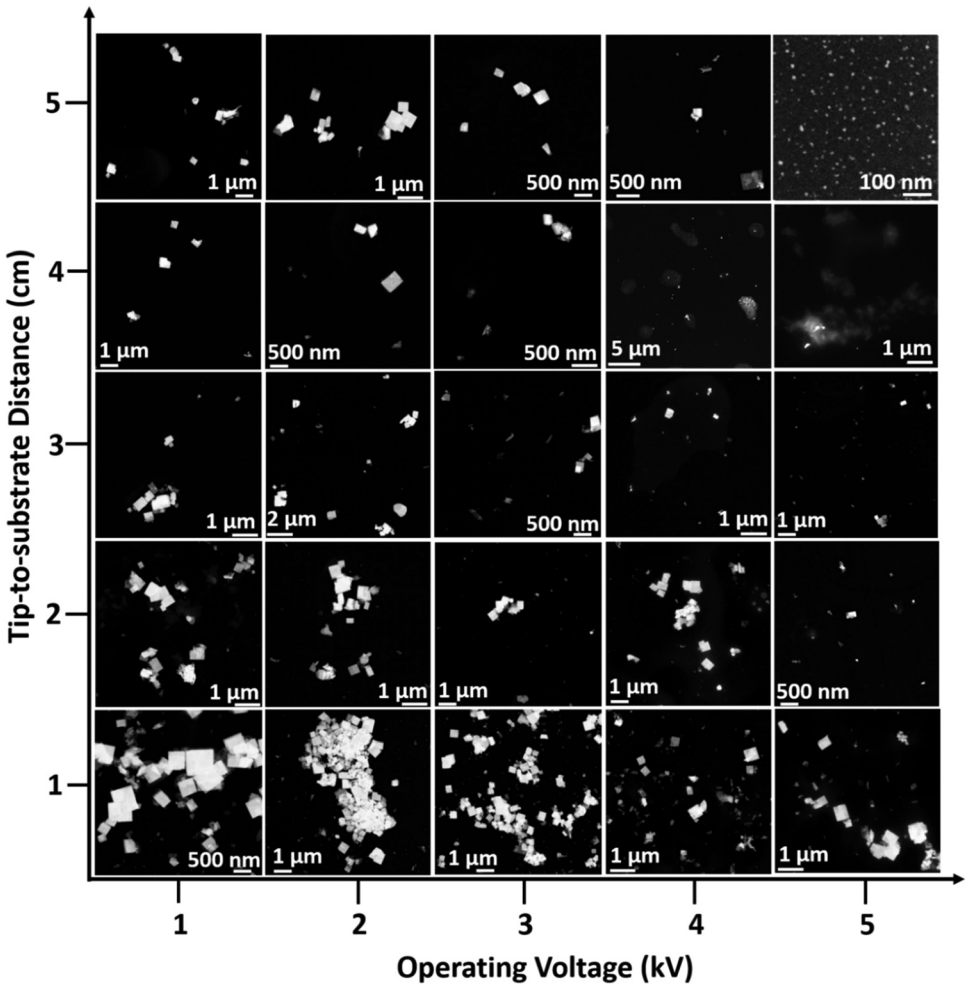

Fig. 2 Large area HAADF-STEM images showing the disintegration pathway of two-dimensional WS_2 sheets to particles as a function of applied potential (in kV) and tip-to-substrate distance (in cm). The applied potential was varied from 1 to 5 kV and the tip-to-substrate distance was varied from 1 to 5 cm. The potential and distance values for an experiment correspond to the centre of the HAADF-STEM image. As can be seen, large *L* and *V* result in nanoparticles. Corresponding bright-field images are shown in Fig. S4.

and local crystallographic order, which are essential for possible catalytic and electronic applications, are preserved throughout the size-reduction process. We believe that in the observed microdroplet mechanochemistry,[34] preferably the basal plane slippage is taking place, followed by edge plane cleavage.

Raman spectroscopy was used to investigate the structural integrity and phase purity of the synthesized WS_2 nanoparticles, in comparison with the bulk and few-layer 2D materials. To obtain the Raman spectrum of WS_2 nanoparticles, we have electrosprayed the few-layer 2D material (Fig. 1b) at (5,5) for 18 h on an indium tin oxide (ITO) glass slide (Fig. S11g). All three samples exhibited the two characteristic vibrational modes of the 2H phase: the in-plane E^1_{2g} and the out-of-plane A_{1g} modes, confirming that the 2H crystal structure is preserved throughout the transformation from bulk to few-layer sheets and finally to nanoparticles (Fig. 3 and Fig. S11).[35,36] The E^1_{2g} mode shows a systematic variation in intensity across the three samples, *i.e.*, the highest in the few-layer two-dimensional sheets, intermediate in the bulk, and the lowest in the nanoparticles, which can be attributed to enhanced resonance Raman scattering in the few-layer sheets due to their reduced dimensionality and modified electronic structure,[37] while the decreased intensity in nanoparticles reflects increased phonon scattering from surface defects, edge sites, and reduced crystallite size.[38] In contrast, the A_{1g} mode shows no appreciable change in intensity across the three samples, suggesting that although there is a change in the number of layers, the local W–S bond environment is largely unaffected by the lateral size reduction.[35] Regarding peak broadening, both the E^1_{2g} and A_{1g} modes do not follow the same trend as intensity. The observed broad peaks for the few-layer sheets can be attributed to the presence of stacking disorder, interlayer coupling inhomogeneity, and increased sensitivity to local environmental fluctuations that arise when the bulk WS_2 is converted to the few-layer regime *via* water exfoliation.[36,39] As the particles transition from bulk to 2D nanosheets and finally to nanoparticles, the FWHM of the E^1_{2g} mode changes respectively from 21.5 to 21.6 to 13.1 cm^{-1}. Similarly, for the A_{1g} mode, the FWHM

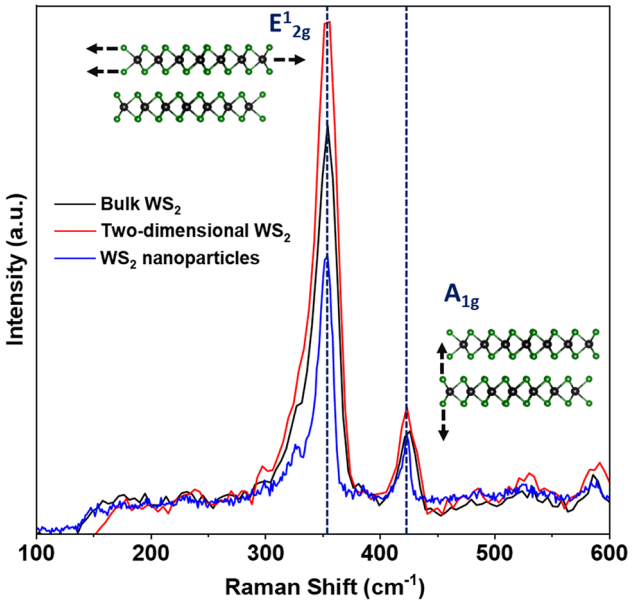

Fig. 3 Raman spectra of bulk WS_2, two-dimensional sheets of WS_2 and WS_2 nanoparticles.

changes significantly, from 15.4 (bulk) to 16.1 (2D sheets) and finally to 8.0 cm^{-1} (nanoparticles). The narrowest linewidths observed in the nanoparticles, despite their nanoscale dimensions, suggest that the controlled local environment of the microdroplet-based synthesis route minimizes the introduction of structural defects and strain.[38] Importantly, the peak positions of both the E^1_{2g} and A_{1g} modes remain consistent across all three samples with no observable Raman shift, confirming the absence of phase transformations during the synthesis process, providing strong evidence that the 2H polymorph is fully retained in the nanoparticles during microdroplet mechanochemistry, which is difficult to achieve in conventional methods as mentioned earlier.

In summary, we have demonstrated that charged water microdroplets generated by electrospray can drive stepwise disintegration of two-dimensional WS_2 sheets into nanoparticles under ambient conditions, with the applied voltage and tip-to-substrate distance serving as key parameters governing lateral size control. Crucially, the 2H crystal phase is fully preserved throughout the transformation, establishing a mild and scalable route to phase-pure WS_2 nanoparticles. These findings highlight the potential of charged water microdroplets as a versatile platform for ambient nanomaterial synthesis and open new directions for phase-preserved size reduction of other layered transition metal dichalcogenides. By implementing a high-throughput multi-nozzle electrospray setup, scalability can also be achieved.

Author contributions

K. K. and T. P. proposed the problem and suggested necessary experiments. K. K. performed all experiments, including synthesis and characterization. S. M. performed Raman measurements. A. S. helped with transmission electron microscopy measurements. A. M. performed scanning electron microscopy. T. P. supervised the research. K. K. and T. P. discussed the results and wrote the manuscript.

Conflicts of interest

There are no conflicts to declare.

Data availability

The data supporting this article are included in the main article and its supplementary information (SI). Supplementary information is available. See DOI: https://doi.org/10.1039/d6cc03938c.

No additional data have been deposited in external repositories.

Acknowledgements

The authors thank the Anusandhan National Research Foundation (ANRF), Department of Science and Technology (DST), University Grants Commission (UGC), Government of India and the Centre of Excellence on Molecular Materials and Functions under the Institution of Eminence Scheme of IIT Madras for generous funding and supporting the research on nanomaterials. The authors thank Dr. Depanjan Sarkar for helpful comments. T. P. thanks ANRF for a JC Bose Fellowship. TEM measurements were collected at the ANRF National Facility for Cryo-Electron Microscopy at IIT Madras.

References

1 H. R. Gutiérrez, N. Perea-López, A. L. Elías, A. Berkdemir, B. Wang, R. Lv, F. López-Urías, V. H. Crespi, H. Terrones and M. Terrones, *Nano Lett.*, 2013, **13**, 3447–3454.
2 A. N. Enyashin, L. Yadgarov, L. Houben, I. Popov, M. Weidenbach, R. Tenne, M. Bar-Sadan and G. Seifert, *J. Phys. Chem. C*, 2011, **115**, 24586–24591.
3 Y. Yao, Z. Jin, Y. Chen, Z. Gao, J. Yan, H. Liu, J. Wang, Y. Li and S. (Frank) Liu, *Carbon N. Y.*, 2018, **129**, 228–235.
4 J. Singh, R. Sebait, P. Raj Adhikari, D. Dridi Khushboo, N.-N. Vu, R. Soni and P. Nguyen-Tri, *ACS Appl. Nano Mater.*, 2025, **8**, 14607–14621.
5 L. Joly-Pottuz, F. Dassenoy, M. Belin, B. Vacher, J. M. Martin and N. Fleischer, *Tribol. Lett.*, 2005, **18**, 477–485.
6 S. Sengupta and M. Kundu, *ChemistrySelect*, 2020, **5**, 14183–14189.
7 K. Kundu, D. C. Binwal, P. Vishnoi and C. N. R. Rao, *Chem. – Eur. J.*, 2026, e71188.
8 M. A. Lukowski, A. S. Daniel, F. Meng, A. Forticaux, L. Li and S. Jin, *J. Am. Chem. Soc.*, 2013, **135**, 10274–10277.
9 R. Scarfiello, A. Cesari, D. Altamura, S. Masi, C. Nobile, F. Balzano, C. Giannini, V. Grillo, A. H. Tavabi, R. E. Dunin-Borkowski, G. Uccello-Barretta, P. D. Cozzoli and A. Rizzo, *Nanoscale Adv.*, 2019, **1**, 2772–2782.
10 S. Cao, T. Liu, S. Hussain, W. Zeng, X. Peng and F. Pan, *Mater. Lett.*, 2014, **129**, 205–208.
11 P. Chavalekvirat, W. Hirunpinyopas, K. Deshsorn, K. Jitapunkul and P. Iamprasertkun, *Precis. Chem.*, 2024, **2**, 300–329.
12 C. Ghosh, M. K. Singh, S. Parida, M. T. Janish, A. Dobley, A. M. Dongare and C. B. Carter, *Sci. Rep.*, 2021, **11**, 9014.
13 X. Wang, J. Dan, Z. Hu, J. F. Leong, Q. Zhang, Z. Qin, S. Li, J. Lu, S. J. Pennycook, W. Sun and C. H. Sow, *Chem. Mater.*, 2019, **31**, 7970–7978.

14 S. X. Leong, C. C. Mayorga-Martinez, X. Chia, J. Luxa, Z. Sofer and M. Pumera, *ACS Appl. Mater. Interfaces*, 2017, **9**, 26350–26356.
15 J. Yan, S. Lian, Z. Cao, Y. Du, P. Wu, H. Sun and Y. An, *Vacuum*, 2023, **207**, 111564.
16 L. Maduro, S. E. van Heijst and S. Conesa-Boj, *ACS Phys. Chem. Au*, 2022, **2**, 191–198.
17 P. Chithaiah, D. Chandra Binwal, S. Mallick and C. N. R. Rao, *Zeitschrift für Anorg. und Allg. Chemie*, 2024, **650**, e202400035.
18 H. Xiong, J. K. Lee, R. N. Zare and W. Min, *J. Phys. Chem. Lett.*, 2020, **11**, 7423–7428.
19 H. Hao, I. Leven and T. Head-Gordon, *Nat. Commun.*, 2022, **13**, 280.
20 Z. Wei, Y. Li, R. G. Cooks and X. Yan, *Annu. Rev. Phys. Chem.*, 2020, **71**, 31–51.
21 S. Banerjee and R. N. Zare, *Angew. Chem.*, 2015, **127**, 15008–15012.
22 J. Zhou, Q. Wang, G. Cheng, W. Shen, R. N. Zare and X. Sun, *J. Am. Chem. Soc.*, 2025, **147**, 10916–10924.
23 B. K. Spoorthi, K. Debnath, P. Basuri, A. Nagar, U. V. Waghmare and T. Pradeep, *Science*, 2024, **384**, 1012–1017.
24 P. Patidar, A. Mahapatra, B. Soni, S. Chowdhury, S. Manna, A. R. Kini, A. Som, D. Sarkar and T. Pradeep, *Nanoscale*, 2026, **18**, 11763–11768.
25 J. Sulthana, A. Mahapatra, M. Bhan, D. Sarkar and T. Pradeep, *J. Phys. Chem. C*, 2026, **130**, 5007–5015.
26 S. Gupta, R. B. Sankar, A. Som, K. Unni, S. Manna, P. Patidar, D. Sarkar and P. Thalappil, *Small Struct.*, 2026, **7**, e70414.
27 A. Mahapatra, A. Som, B. K. Spoorthi, D. Sarkar and T. Pradeep, *Chem. Commun.*, 2025, **61**, 15846–15849.
28 H. Schweiger, P. Raybaud, G. Kresse and H. Toulhoat, *J. Catal.*, 2002, **207**, 76–87.
29 L. Meng, J. Feng, Y. Yu, W. Yan, H. Li, X. Wang and X. Yan, *Phys. E*, 2019, **114**, 113641.
30 D. S. Gavhane, A. D. Sontakke and M. A. van Huis, *Adv. Funct. Mater.*, 2022, **32**, 2106450.
31 E. Ringe, R. P. Van Duyne and L. D. Marks, *J. Phys. Chem. C*, 2013, **117**, 15859–15870.
32 S. Yamashita, J. Kikkawa, K. Yanagisawa, T. Nagai, K. Ishizuka and K. Kimoto, *Sci. Rep.*, 2018, **8**, 12325.
33 S. J. Pennycook and L. A. Boatner, *Nature*, 1988, **336**, 565–567.
34 T. Pradeep, *ACS Sustainable Chem. Eng.*, 2026, **14**, 25–30.
35 A. Berkdemir, H. R. Gutiérrez, A. R. Botello-Méndez, N. Perea-López, A. L. Elías, C.-I. Chia, B. Wang, V. H. Crespi, F. López-Urías, J.-C. Charlier, H. Terrones and M. Terrones, *Sci. Rep.*, 2013, **3**, 1755.
36 B. Rajeswaran, R. Konar, R. Yitzhari, G. D. Nessim and Y. R. Tischler, *J. Raman Spectrosc.*, 2023, **54**, 1030–1037.
37 A. P. S. Gaur, S. Sahoo, J. F. Scott and R. S. Katiyar, *J. Phys. Chem. C*, 2015, **119**, 5146–5151.
38 S. V. Koniakhin, O. I. Utesov and A. G. Yashenkin, *Diamond Relat. Mater.*, 2024, **146**, 111182.
39 K. S. Novoselov, D. Jiang, F. Schedin, T. J. Booth, V. V. Khotkevich, S. V. Morozov and A. K. Geim, *Proc. Natl. Acad. Sci.*, 2005, **102**, 10451–10453.